3D Visualization of High-Resolution ILI Caliper Data: A Systematic Framework for Fitness-For-Service Assessment of Pipeline Wrinkles

Kachi Ndubuaku[1], Brendan Eirich[2], Kristian Olsen[3]
[1]Enbridge, [2]ATCO, [3]Stantec

Organized by
CLARION
TECHNICAL CONFERENCES

https://doi.org/10.52202/078572-0044

https://doi.org/10.52202/078572-0044

Abstract

Mild ripples may be introduced in pipelines prior to installation, during the process of forming field bends. Wrinkles/buckles may also develop in pipelines under monotonic displacement-controlled loading conditions, such as permanent ground deformation. Many pipeline industry codes define the acceptability of surficial deformations in energy pipelines based on generic serviceability limit criteria such as adverse effects of wrinkles on the integrity of pipe coating or impairment of in-line inspection. However, the codes do not provide explicit guidance on the acceptance standards with regards to the effect of surficial deformations on the structural/mechanical performance and long-term integrity of pipelines. A powerful transformation tool is presented in this paper to approximate the deformed centerline profile, as well as surface deformities, of pipelines using high-resolution ILI IMU/caliper data. The tool provides interactive 3D visualization of the deformed pipeline therefore allowing proper categorization of the observed deformities, and also evaluates the longitudinal and circumferential bending strains over the full pipeline surface. The tool also generates the 3D surface mesh needed as input for more advanced finite element analysis (FEA), including pipe-soil interaction properties required to properly simulate buried conditions if applicable. Ultimately, a systematic approach is outlined herein for using the analytical strain estimates generated by the transformation tool, combined with the results of FEA, as input for performing level 3 fitness-for-service fatigue-life assessment of wrinkled pipelines.

Introduction

During routine In-Line Inspection (ILI), ATCO discovered 47 wrinkle bends on a section of its mid-1940's vintage NPS16 (406.4 mm diameter) transmission pipeline near Edmonton, Alberta. The line is predominantly seamless 9.5mm W.T. API 5L Grade B pipe and was manufactured by the Scottish pipe mill, Stewarts & Lloyds. It transports sweet, dry natural gas at a licensed MOP of 4030 kPa. These wrinkle features are assumed to be purposefully installed as shallow bends and have been present since the line's original construction. The indicated wrinkle features were previously assessed to be outside the acceptable screening limits specified in Section 10.10.8.3 of CSA Z662-19 without additional engineering assessment. As a result, ATCO required a more detailed engineering assessment to evaluate the severity and fitness-for-service characteristics of the wrinkle-bend features in the pipeline and determine which features may require permanent repair.

Figure 1 shows a cut-out from a section of the line which contained two wrinkles that were designed as part a wrinkle bend. The maximum effective strain in this cutout was calculated by a 3rd party per ASME B31.8R to be 17.4% at the crest of the more severe wrinkle.

https://doi.org/10.52202/078572-0044

Figure 1: Transmission line cut-out

Background

Modern ILI tools utilize a wide variety of technologies to measure the current state of pipeline integrity. One such technology is caliper data, which employs a radial array of rocker arms that travel along the pipeline length and detect radial deviations in pipeline geometry. The process starts with radius measurements at discrete "o'clock" positions along the pipeline circumference which are mapped as the ILI tool travels along the pipeline. These radial deviation values must then be converted to a continuous surface map, and finally converted into strain values. Pipeline codes such as CSA Z662 provide guidance on the maximum-allowable strain. Such codes also refer to industry standards and best-practices which allow integrity engineers to determine strain-induced operating risk. In all cases, strain created by pipeline surface deviations elevate operating risk, and an efficient and accurate strain visualization and calculation tool can greatly enhance rapid screening of pipeline sections that require detailed analysis and/or direct inspection via pipeline digs.

Wrinkles are typically initiated due to localized buckling of the pipe wall under externally applied loading. Historically, they have also been formed from straight pipe joints to create shallow bends in the pipe alignment. The geometry of the wrinkle is strongly influenced by the loading conditions responsible for buckling the pipe.

Evaluation of the wrinkle bends was completed through three main tasks:

1. Geometric (caliper and IMU) data obtained from an ILI vendor was used to create a 3D mesh approximation of the wrinkled pipe surface using cubic spline interpolation methods. The caliper data row intervals and interpolated surface mesh grid spacing required to produce an approximation of the wrinkled pipe surface was calibrated using strain evaluation results

https://doi.org/10.52202/078572-0044

obtained from a small subset of NDE laser scan data from excavations conducted by ATCO and assessed by another inspection company. Longitudinal, circumferential, and equivalent strains were derived from the interpolated spline surface based on ASME B31.8R.

2. The interpolated surface provided the nodal coordinates for direct input into the creation of shell elements in the finite element (FE) models. FE models were created using the commercially available FE package, ABAQUS CAE 2019. Wrinkled areas of the pipeline, including sufficient pipe length offsets upstream and downstream of the most severe point (MSP), were modelled using ABAQUS S4R shell elements while pipe sections beyond the wrinkled areas, upstream and downstream, were modelled using ABAQUS PIPE32 beam elements. Beam elements were included to capture additional bending moment contribution of adjacent non-straight pipe sections. Pipe-soil interaction was also modelled using ABAQUS 3D connector springs (CONN3D2) compatible with the S4R elements and ABAQUS 3D pipe-soil interaction elements (PSI36) compatible with the PIPE32 elements. Respective operational parameters and successive loading cases were applied to the FE pipe model through three cycles of operation to verify non-existence of ratcheting in the models.

3. The maximum shear and associated normal stresses and strains were collated from the results of the FE analysis at all points in the load time history. Rainflow data was derived from two-year pressure-cycling (SCADA) data provided by ATCO and correlated with FEA shear and normal strains. Using the rainflow-correlated maximum shear strain range and the associated normal strain range, the permissible number of reversals (half-cycles) and accumulated fatigue damage over the lifetime of the pipeline (since installation) was calculated using the strain-life equations provided in API 579-2021 clause 14.4.4. Fatigue life knockdown factors per API 579-2021 Table 14.12 were also applied to the remaining life estimates.

The ASME B31.8R strain model is solely based on the surface curvature, hence it is unable to account for through-wall membrane strains in the pipe. However, since the overall strain damage due to pre-operational wrinkle-forming deformation is largely governed by longitudinal strains, the ASME model is considered acceptable for strain damage evaluation as it tends to produce a conservative estimation of the longitudinal strains; the absence of longitudinal membrane strain tends to over-estimate the total (bending plus membrane) longitudinal tensile strain around the intrados of the wrinkle bend where the most severe point of the wrinkles typically exists.

Considering that the two main loading conditions to which the wrinkled pipe is subjected are largely either aligned along the pipe axis (applied bending moment during wrinkle forming) or aligned circumferentially (internal pressure during pipe operation), Stantec selected two corresponding candidate critical planes assumed to be coincident with the through-wall directional (longitudinal and circumferential) stresses and strains in each S4R pipe shell element. This assumption presupposes the non-existence of significant torsional strains or warping deformation of the pipe

https://doi.org/10.52202/078572-0044

which may invalidate the assumption of the longitudinal or circumferential planes as the most critical planes per element.

The fatigue analysis results indicate that the maximum longitudinal net fatigue damage (LNFD, i.e., here the candidate critical plane is circumferential so that the normal strain is longitudinal) is generally higher than the maximum circumferential net fatigue damage (CNFD, i.e., where the candidate critical plane is longitudinal so that the normal strain is circumferential) whereas the remaining fatigue life (RFL) is generally less in the circumferential direction than in the longitudinal direction. This supports the expectation that the net fatigue damage (NFD) is driven by the severe longitudinal strains induced in the pipe during the wrinkle-forming process whereas the RFL is driven more by the cyclic circumferential stresses induced by fluctuating pressurization during the operation of the pipeline. This invariably also suggests that the CNFD will likely overtake the LNFD as the pipeline approaches the end of the RFL.

By ranking the wrinkle features according to severity of LNFD, five features (#02-016, #09-390, #10-155, #10-297, and #19-251) recorded a maximum LNFD greater than 1%. Three other features (#14-124, #14-139, and #14-151) recorded a maximum LNFD less than 1% but greater than 0.95%. Using the lower-bound Ductile Failure Damage Indicator (DFDI) criteria, five features (#09-390, #10-155, #14-124, #14-139, and #19-251) recorded a maximum DFDI greater than 95%. However, going by the upper-bound DFDI criteria, sixteen features (#03-402, #08-238, #08-299, #09-390, #10-155, #10-200, #10-211, #10-383, #12-159, #13-192, #14-124, #14-139, #14-151, #18-132, #18-317, and #19-251) recorded a maximum DFDI greater than 95%. For all the wrinkle features, the lowest RFL calculated is greater than a 100-year cut-off limit that was set as the acceptance threshold for fatigue life.

In addition to the fatigue-life evaluation, the fitness-for-service assessment approach detailed in API RP 1183 Section 8 was also applied to determine the potential for crack initiation in the pipe wall during the wrinkle forming process. The Ductile Failure Damage Indicator (DFDI) crack formation strain model was used to provide a simple severity ranking of all the wrinkle features assessed.

While all the features assessed pass the accumulated fatigue damage criteria (NFD < 100%), close attention should be paid to the features that have significantly high wrinkle-forming strains, especially those five features with a lower-bound DFDI greater than 95% (i.e., #09-390, #10-155, #14-124, #14-139, and #19-251), especially since all five features also recorded a maximum LNFD greater than 0.95%. Of all 47 features assessed in this report, 2 features (#02-016 and #10-297) present a somewhat peculiar scenario whereby, compared to all other features, the lower-bound DFDI is relatively low (52.2% and 29.9%) whereas the LFND is relatively high (2.8% and 1.4%). It is also interesting to note that the CNFD for both features (#02-016 and #10-297) is also significantly high (1.4% and 1.1%) - which is approximately 5090% and 4082%, respectively, of the average CNFD for the remaining 45 features assessed in this report. This result is believed to indicate the likelihood of

https://doi.org/10.52202/078572-0044

significant shear strains in the pipe which would further reduce the permissible number of half cycles under cyclic pressure loading.

Stantec also applied the ASME B31.8R model to evaluate the wrinkle-forming strains in the wrinkle features. Stantec further created hybrid beam-shell FE models of the wrinkle features using IMU and caliper data provided by ATCO. The FE models allowed Stantec to simulate a few operational cycles guided by SCADA pressure-cycling data provided by ATCO, and subsequently perform fatigue strain life evaluation of the wrinkle features as per API 579 (2021)-14.4.4.

The objective of this assessment is to evaluate the strain history of 47 wrinkle features within the segment of interest of the pipeline, and to perform strain-life fatigue evaluation to determine the mechanical integrity of each wrinkle feature with respect to suitability for continued service as currently licensed. Achieving the objectives involves the following tasks:

1. Reviewing existing documentation to support the project. Collating the following data required to evaluate the wrinkle-forming strains, as well as to develop FE models: geometric (caliper and IMU) pipe tally/pipe book, material, and operational parameters (pressure-cycling history from SCADA data),

2. Processing input data and apply cubic spline interpolation methods to generate refined 3D surface mesh of wrinkled features, including nodal coordinates to be imported into ABAQUS for generation of FE models,

3. Deriving the spline curvature along the generated 3D surface of the wrinkled features and estimating the longitudinal, circumferential, and effective strains at each node of the wrinkled surface,

4. Applying respective operational parameters and successive loading cases to the FE pipe model. Apply up to three cycles of operation to verify non-existence of ratcheting in model. Output maximum shear strains, and associated longitudinal/circumferential strains as candidate-plane normal strains, for all points in the load time history,

5. Performing rainflow counting on pressure-cycling data and correlate rainflow data with shear and candidate-plane normal strains. Calculate the maximum shear strain ranges and the associated normal strain and determine the permissible number of reversals (half-cycles),

6. Computing the accumulated fatigue damage for the loading time history based on the duration provided by the SCADA data using Miner's rule.

https://doi.org/10.52202/078572-0044

Purpose, Scope, and Assumptions

Modelling

The commercially available finite element (FE) package SIMULIA Abaqus 2019 (Abaqus/Standard) was used to perform a quasi-static non-linear elastic-plastic-material analysis with the large deformation (non-linear geometry) setting enabled. A combination of connector elements and pipe-soil interaction (PSI) elements were also utilized to adequately simulate the buried conditions of the pipeline in soil.

An approximately 3-meter-section (1.5 meters upstream and 1.5 meters downstream) of pipe immediately adjacent to each wrinkle was modelled using Abaqus S4R shell elements. Nodal coordinates of the shell mesh were generated by trigonometric revolution of radial vectors around the IMU centerline coordinates of the pipeline. Pipe-soil interaction was modelled for the S4R shell elements using three-dimensional connector springs (CONN3D2) in 6 independent directions. Each spring direction was tied (and distributed) to collective surfaces on the exterior of the shell elements such that only the exterior surfaces that are facing the direction of relative motion of the pipe with respect to the soil are engaged. The axial soil springs were also modelled to uniformly engage the entire pipe circumference in traction.

While the wrinkle and immediately adjacent sections of pipe are the primary regions of interest for the assessment, it is necessary to establish adequate virtual anchors at a sufficient distance away from the wrinkled regions in the pipe models. The pipe sections upstream and downstream of the areas modelled with S4R shell elements were thus modelled using 100-meter-sections of Abaqus PIPE32 beam elements. Beam elements are expected to capture additional bending moment contribution of adjacent non-straight pipe sections. Pipe-soil interaction was modelled for the beam elements using three-dimensional 6-node pipe-soil interaction (PSI36) elements compatible with the PIPE32 elements. A screenshot of the hybrid beam-shell pipe model is shown in Figure 2.

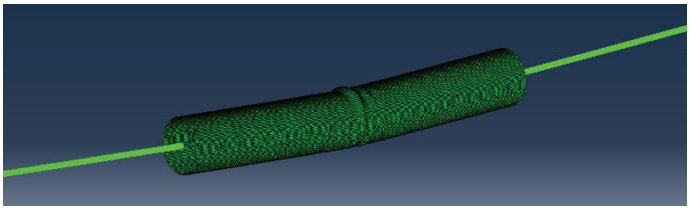

Figure 2. Hybrid beam-shell pipe model

Local coordinate systems were established for each S4R element such that the "11" suffix corresponds to the axial direction and the "22" suffix corresponds to the circumferential direction. The shell mesh was carefully designed such that each shell element has a square shape with dimensions of approximately 9mm × 9mm. At the beam-shell intersections in the pipe model, a reference point with continuum distributing coupling constraint was included to connect the free ends of the shell-

https://doi.org/10.52202/078572-0044

modelled section to the beam-modelled pipe sections. An equivalent concentrated follower load was also applied to each reference point to compensate for the end-cap force generated by internal pressure.

In the FEA models presented in this report, five half-cycle internal pressure quasi-static loading steps were implemented as follows:

Step 1: Apply gravitational loading and internal pressure. The pipeline pressure was ramped up linearly from zero to the defined internal pressure. A maximum pressure of 2123 kPa was recorded from SCADA data, hence a maximum internal pressure of 2500 kPa was applied to the pipe models.

Step 2: Apply operating temperature. The maximum operating temperature (conservatively estimated to be 20°C) was ramped up linearly from the pipeline restraint temperature (0°C).

Step 3: Remove internal pressure. The pipeline pressure was linearly decreased from the maximum internal pressure (2500 kPa) to 0 kPa.

Step 4: Linearly ramp up internal pressure from 0 kPa to 2500 kPa.

Step 5: Decrease internal pressure from 2500 kPa back to 0 kPa.

Step 6: Linearly ramp up internal pressure from 0 kPa to 2500 kPa.

For each proportional internal pressure increment in Step 6 (the final loading step of the FE analysis), the longitudinal and circumferential stresses and strains, as well as the shear strains, in every S4R shell element in the pipe model were extracted and tabulated; to be used for the fatigue strain life calculations.

Modelling Pipe-Soil Interaction

The wrinkled regions of the pipe models were modelled using Abaqus S4R shell elements while the pipe sections that extend beyond the wrinkled regions of the pipe were modelled with Abaqus PIPE32 beam elements. The soil surrounding the pipe was modelled as bi-linear springs using Abaqus Pipe-Soil Interaction (PSI36) elements in the beam-modelled areas and Abaqus Connector (CONN3D2) elements in the shell-modelled wrinkled regions. Each pipe-soil interaction element operates in six directions on each pipe element in the model: axial forward and backward, lateral left and right, and vertical up and down. Figure 3 illustrates the general concept of the pipe-soil interaction springs.

https://doi.org/10.52202/078572-0044

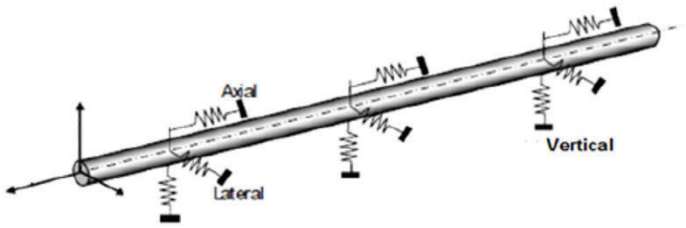

Figure 3: Pipe-soil interaction springs along pipeline

The pipe-soil interaction elements were constrained at the "far-field nodes", while the pipe nodes were connected to the free ends of the pipe-soil interaction elements. This way, the soil supports the pipe as an elastic foundation in all directions. The stiffness of the springs is defined by the axial, lateral, and vertical soil restraints that were determined based on the soil properties. When the pipe moves due to the loads applied from the operating conditions or due to soil movement, the soil springs deflect and either restrain the pipe movement or transfer the displacement of the springs to the pipe. When the pipe displacement is sufficiently large, it displaces the surrounding soil as much as it can surpassing the yield displacement limit of the soil springs, after which the bi-linear soil springs will transition into the perfectly plastic regime limiting the developed soil-structure interaction forces to a maximum value.

Results and Discussion

ASME Strain Model Calibration

The ASME B31.8R strain model was originally developed for analyzing dents; hence, to validate the applicability of the AMSE strain equations for assessing wrinkle strains, a simple FE model was defined by applying end-rotation to a short pipe stub (diameter = 400mm; length = 1000mm) until a ripple was formed. The validation FE model was formed using S4R shell elements with linear-elastic material and large deformation (non-linear geometry) setting enabled. Comparison between the circumferential and longitudinal strains obtained from the ASME 31.8R strain model and those obtained from the FE model are shown in Figure 4 and 6.

https://doi.org/10.52202/078572-0044

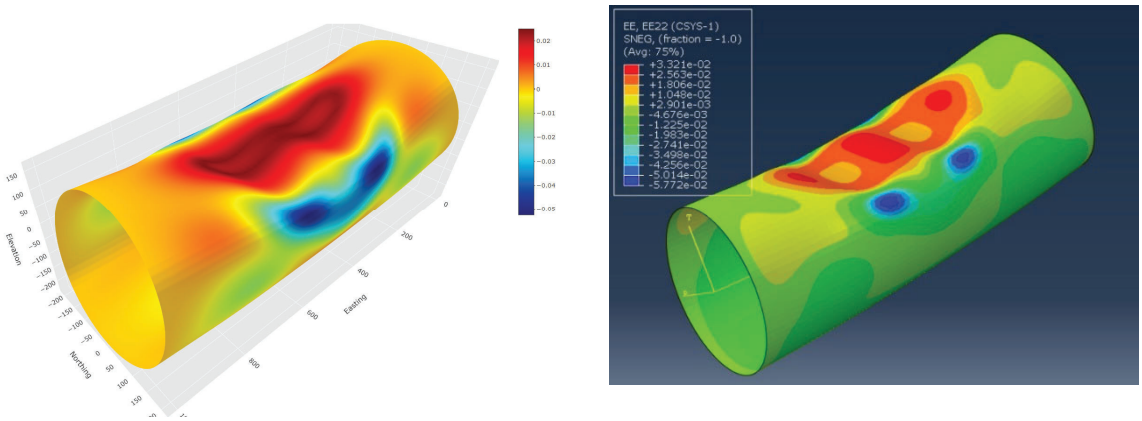

Figure 4. Pipe model calibration (FE vs ASME model comparison – circumferential strains)

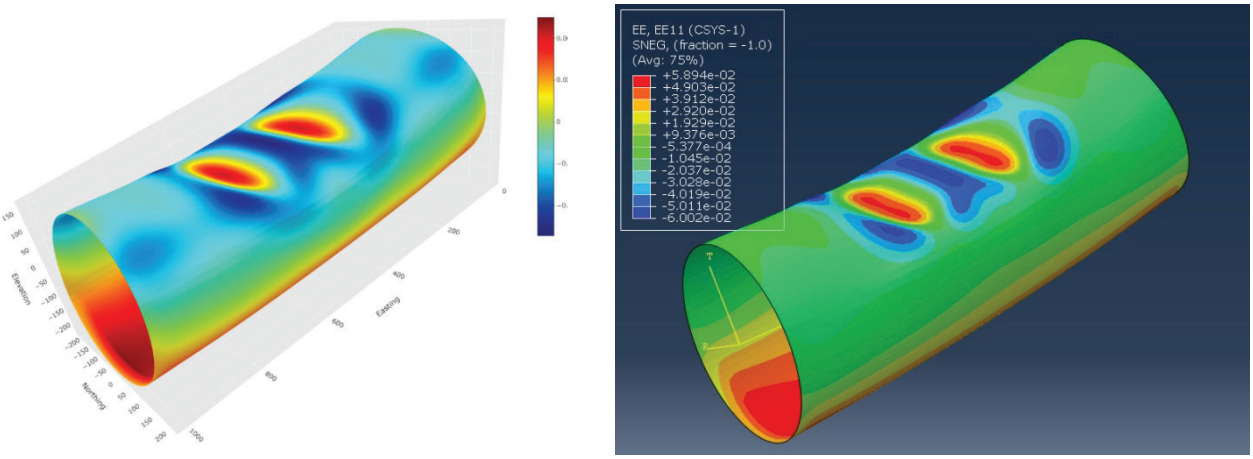

Figure 5. Pipe model calibration (FE vs ASME model comparison – longitudinal strains)

Caliper Data Smoothing

It is necessary to infer a reasonably-smooth approximation of the pipe surface from the caliper data since the estimated strains are highly sensitive to the localized curvature at every point on the pipe surface. Calibrating the filter parameters required to reduce the inherent noise in the caliper data relied on laser scan data from NDE conducted by Acuren on behalf of ATCO. Caliper data smoothing was achieved using the signal processing elliptic filtering method; a fifth-order low-pass filter which is effective for attenuating unwanted frequency components from signal-like data. An additional noise-smoothing technique applied to the caliper data was achieved by extracting the original caliper data at row intervals greater than 1. Equivalent strains obtained from the laser scan data are compared with the strains obtained from caliper data as shown in Figure 6 and 8.

https://doi.org/10.52202/078572-0044

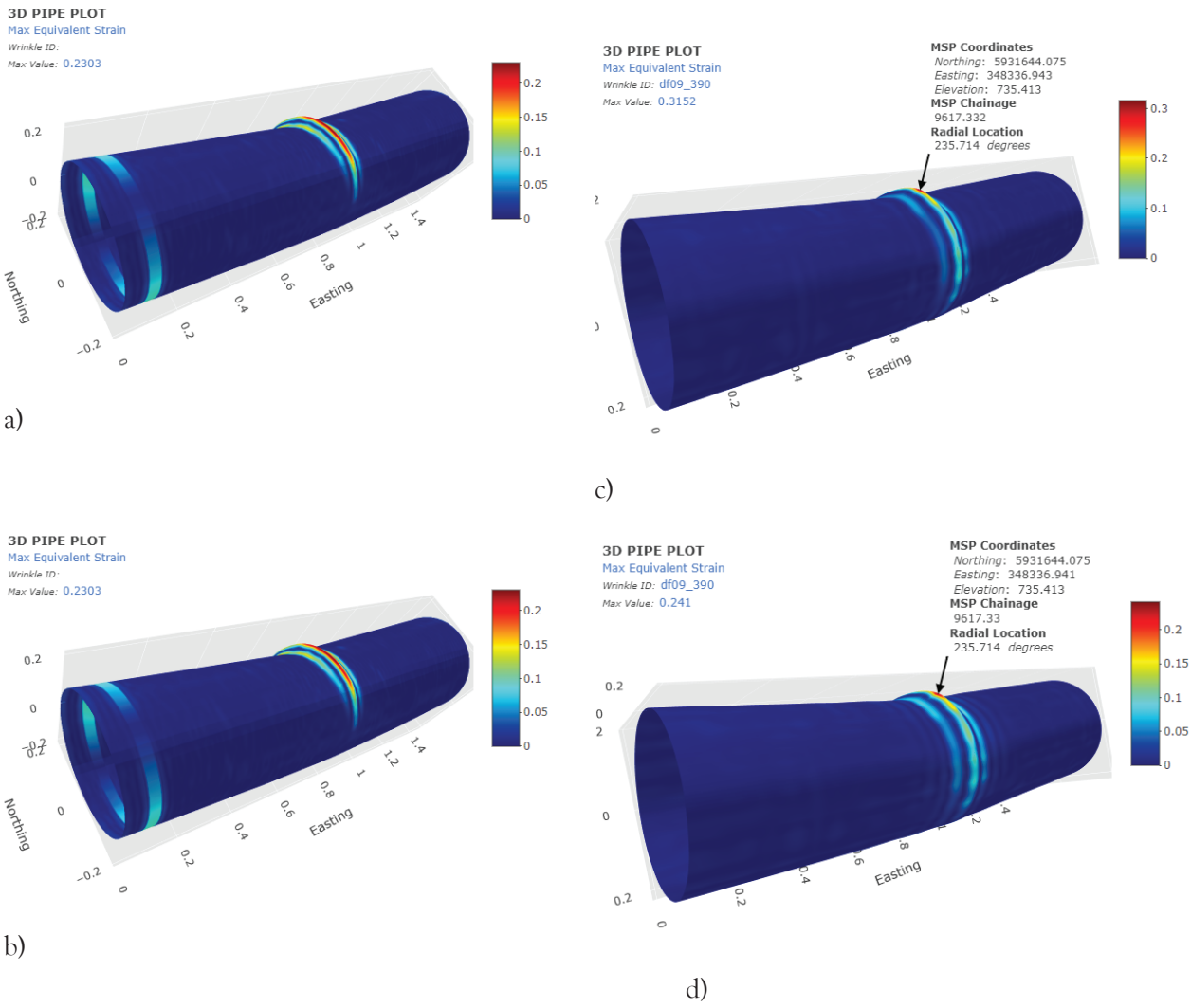

Figure 6. Equivalent strains comparison (laser scan vs caliper data – wrinkle #09-390), (a) equivalent strain for 2-row-interval laser scan data, (b) equivalent strain for 4-row-interval laser scan data, (c) equivalent strain for 2-row-interval caliper data, (d) equivalent strain for 3-row-interval caliper data

https://doi.org/10.52202/078572-0044

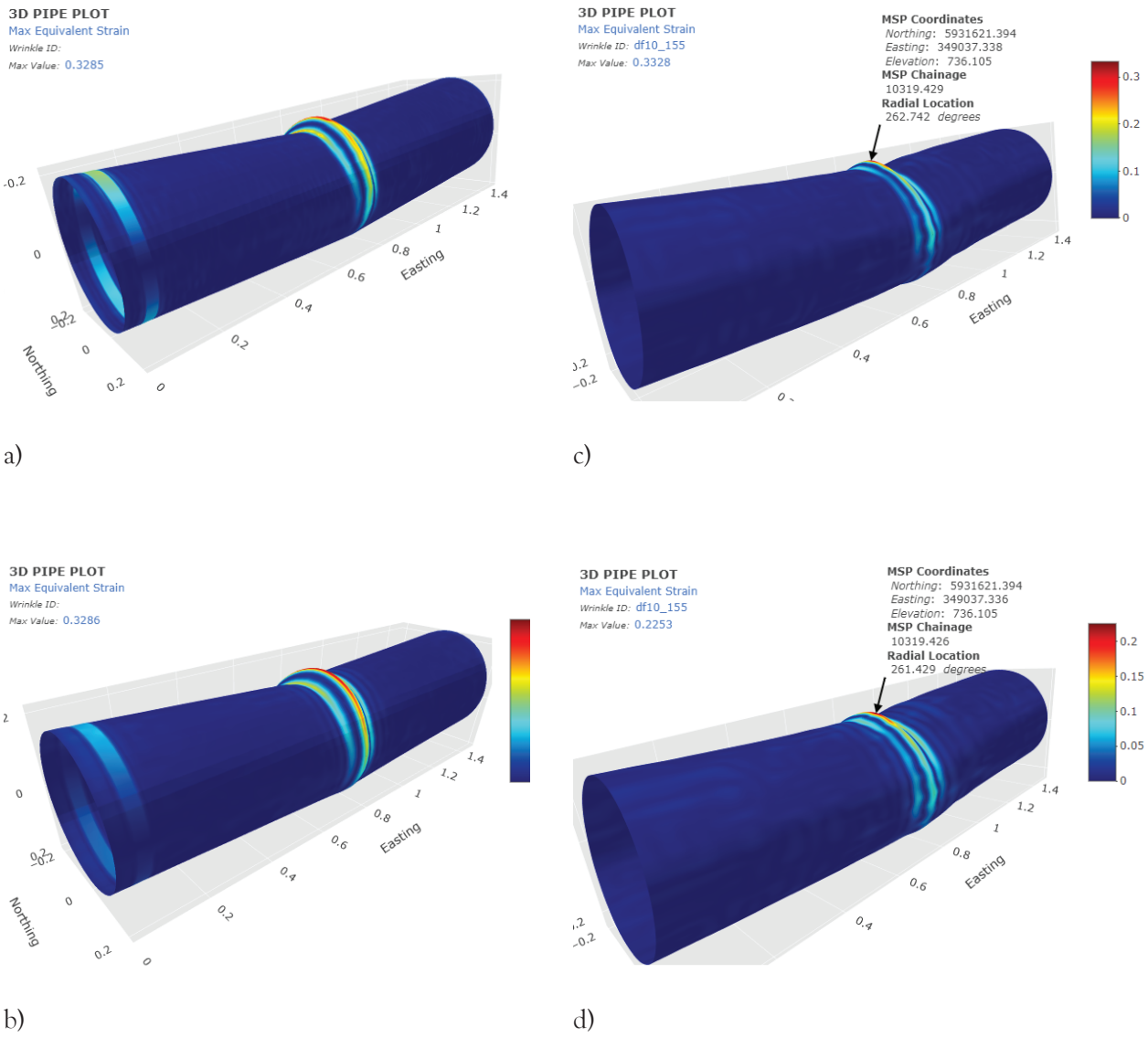

Figure 7. Equivalent strains comparison (laser scan vs caliper data – wrinkle #10-155), (a) equivalent strain for 2-row-interval laser scan data, (b) equivalent strain for 4-row-interval laser scan data, (c) equivalent strain for 2-row-interval caliper data, (d) equivalent strain for 3-row-interval caliper data

From the laser scan plots in Figure 6(a) and Figure 6(b), it is evident that, for Wrinkle #09-390, using a finer mesh (2-row-interval) produces a higher maximum equivalent strain compared to the coarser mesh (4-row-interval) which produces a lower maximum equivalent strain. The caliper data plots also indicate that the finer mesh (2-row-interval) produces a higher maximum equivalent strain than the coarser mesh (3-row-interval). On the other hand, for Wrinkle #10-155 (as shown in Figure 7(a) and Figure 7(b)), while the caliper data plots produce a higher maximum equivalent strain for the finer mesh (2-row-interval) compared to the coarser mesh (3-row-interval), the mesh size of the laser scan plots shows a negligible effect on the maximum equivalent strains.

https://doi.org/10.52202/078572-0044

The average value of the laser scan maximum equivalent strain for Wrinkle #09-390 is 22.38% while that of Wrinkle #10-155 is 32.86%. For Wrinkle #09-390, the caliper data overestimates the laser scan maximum equivalent strain by 40.84% for the finer mesh while the coarser mesh underestimates the laser scan maximum equivalent strain by 2.95%; whereas, for Wrinkle #10-155, the caliper data overestimates the laser scan maximum equivalent strain by 1.28% for the finer mesh while the coarser mesh underestimates the laser scan maximum equivalent strain by 31.44%.

Since the two laser scan data used for calibration are insufficient to statistically infer the better model, the more conservative option (the finer mesh, i.e., the 2-row-interval caliper data) was determined as more acceptable for assessing the wrinkle-forming strains and fatigue life of all the wrinkle features presented in this report.

Wrinkle-Forming Strains

The strains induced in the pipe during the wrinkle-forming process were assessed using the ductile failure damage indicator (DFDI) crack formation strain model described in API RP 1183 Section 8.2.2. The DFDI was originally developed to evaluate the total plastic damage in pipe dents due to large plastic deformation. API RP 1183 Equation (22) provides a simplified procedure to estimate the DFDI based on geometric approximations of the wrinkle features without requiring a detailed FEA model. The simplified procedure specifies the upper and lower bounds of the DFDI whereby the upper bound DFDI assumes a biaxial loading condition ($\sigma_1 \neq 0$, $\sigma_2 = \sigma_1$, $\sigma_3 = 0$) and the lower bound DFDI assumes a uniaxial loading condition ($\sigma_1 \neq 0$, $\sigma_2 = 0$, $\sigma_3 = 0$). API RP 1183 indicates that the material's critical strain parameter ε_o is usually in the range of 0.3 to 0.6 for typical pipeline steels; hence, the lower bound value ($\varepsilon_o = 0.3$) was applied to the formulas in API RP 1183 Equation (22) to derive the DFDI estimates for the wrinkle features assessed in this report. The derived lower- and upper-bound DFDI estimates, ranked in descending order of magnitude for all the wrinkle features with upper-bound DFDI > 95%, are shown in Table 2.

It is expected that using the lower bound value of the critical strain parameter ($\varepsilon_o = 0.3$) produces overly conservative results for the upper-bound DFDI criteria. Hence, the lower-bound DFDI estimates presented in Table 3 are considered more realistic than the upper-bound estimates. Severity ranking of the lower-bound DFDI estimates indicates that five features (#09-390, #10-155, #14-124, #14-139, and #19-251) are above 95% and are, thus, considered the most prone to crack initiation.

Considering that this segment of the pipeline has been in operation since 1951, it is likely that no significant cracks were initiated during the wrinkle-forming process at any of these 5 wrinkle features, as no leaks have been reported since installation. However, magnetic particle inspection (MPI) found mill scabs along large portions of the external surface of one of the wrinkles previously excavated. A small amount of scale build-up and minor corrosion damage was also observed at the internal surface. There was, however, no evidence of crack growth or corrosion within the mill scabs, according to the MPI. Nonetheless, the DFDI does not account for microstructural imperfections, and may therefore underestimate the true extent of strain damage. It is also important to remain mindful of any historical incidence or future development of additional strains (especially longitudinally dominant

https://doi.org/10.52202/078572-0044

strains; such as ground movement) which may lead to additional plastic damage and ultimately, cracking.

Strain-Life Evaluation

API 579-2021 Section 14.4.4 provides an overview for a Level 3 Assessment procedure for fatigue evaluation. The Level 3 procedure determines allowable fatigue cycles for a component and its associated loading history using a multiaxial strain-life equation with a mean stress correction - in combination with a critical plane approach. The critical plane approach resolves the stress-strain state at a given point on a number of candidate planes. Fatigue damage is calculated on each candidate plane using the strain-life equation, and the plane with the maximum damage identifies the critical plane and the overall fatigue damage for the given point. The Level 3 Assessment procedure also requires that the entire loading time history covering past and future operation is derived showing the cyclic nature of all applied loadings including thermal gradients. Primary, secondary, and peak strains are then computed, and load pairs are defined for each cycle so that shear and normal strains may be computed.

The full loading history for this assessment was inferred from the pressure-cycling SCADA data obtained from the pipeline over a two-year period (from February 2020 to February 2022). The 2-year SCADA data is presumed to provide an approximate representation of the typical pressure-cycling operation throughout the lifetime of the pipeline. Considering two main modes of loading expected in the pipeline, and to simplify the critical plane approach for this assessment, only two candidate planes were selected: (1) a "circumferential" plane, in which the normal strains are longitudinally oriented, was selected to account for longitudinally-dominant stresses/strains, and (2) a "longitudinal" plane, in which the normal strains are circumferentially oriented, was selected to account for circumferentially-dominant stresses/strains.

The cyclic stress and strain ranges for each element of the FE pipe model was computed based on the pressure amplitudes determined from the SCADA data following the rainflow cycle counting methods defined in API 579-2021 Annex 14C. On each candidate plane, for each cyclic stress range in the loading time history, the maximum shear strain range, $\Delta \gamma_{max,k}$, and the associated normal strain range, $\Delta \varepsilon$ N, were calculated, and the permissible number of reversals (half cycles), $N_{f,k}$, was determined using the Brown-Miller strain-life equation outlined in API 579-2021 Equation 14.75. The Brown-Miller strain-life equation parameters - fatigue strength coefficient (σ _f), fatigue ductility coefficient (ε _f), fatigue strength exponent (b), and fatigue ductility exponent (c) - were applied directly from the values recommended for plain carbon and low-to-medium alloy steels in API 579-2021 Table 14B.2. In computing the fatigue damage, knockdown factors to account for debilitating effects of size, surface finish, environment, and other factors on the fatigue life of the pipeline were applied following the AMSE recommendations from API 579-2021 Table 14.8. Considering the age of the pipeline, surface finish and environmental effects was set to 4.0. Values of 2.5 and 2.0 were

https://doi.org/10.52202/078572-0044

applied for size effect and data scatter respectively thereby leading to a total fatigue life knockdown factor of 20 for the assessment.

Table 1. Wrinkle features (ranked) – upper bound DFDI > 95%

Wrinkle ID	Maximum Equivalent Strain ($\varepsilon_{eq,max}$)	DFDI (lower bound) = $\varepsilon_{eq,max} / \varepsilon_o$	DFDI (upper bound) = 1.65 * $\varepsilon_{eq,max} / \varepsilon_o$
10_155	34.08%	113.60%	187.44%
19_251	31.86%	106.21%	175.25%
14_124	29.15%	97.18%	160.34%
14_139	29.15%	97.16%	160.32%
09_390	28.99%	96.63%	159.44%
14_151	25.52%	85.08%	140.39%
12_159	23.30%	77.67%	128.16%
18_317	22.97%	76.57%	126.33%
10_383	22.88%	76.25%	125.82%
13_192	22.79%	75.97%	125.34%
18_132	22.47%	74.89%	123.57%
08_299	21.10%	70.34%	116.07%
10_200	19.65%	65.51%	108.09%
08_238	19.01%	63.36%	104.54%
10_211	18.93%	63.09%	104.10%
03_402	17.92%	59.73%	98.56%

Results for maximum NFD (longitudinal and circumferential) and minimum RFL (longitudinal and circumferential) are presented in Table 2, ranked according to descending order of severity of the maximum LNFD for wrinkle features with maximum LNFD > 0.95%. Table 2 also includes the contribution of the wrinkle-forming strains to the overall longitudinal NFD (LFND) and the circumferential NFD (CNFD).

In Table 2, the features highlighted in red correspond to the five features (#09-390, #10-155, #14-124, #14-139, #19-251) which recorded a lower-bound DFDI greater than 95%. These five features are considered highest risk with respect to near-term susceptibility to the onset of cracking since they all rank high for both DFDI and LNFD. The other three features (#02-016, #10-297, #14-151) in Table 2 recorded a lower-bound DFDI less than 95% but are still considered medium risk with respect to crack initiation since they have a relatively high ranking for LNFD.

https://doi.org/10.52202/078572-0044

The last two columns in Table 2 indicate that the wrinkle-forming strains have the most significant contribution to both the LNFD and the CNFD. On average the wrinkle-forming strain contribution to NFD is more than 10 orders of magnitude greater than the contribution from pressure-cycling operation in the longitudinal direction, and more than 8 orders of magnitude greater than the contribution from pressure-cycling operation in the circumferential direction. Correlation graphs (with log-scaled vertical axis), collated for all wrinkle features assessed in this report, for maximum wrinkle-forming strains vs max LNFD (total) and maximum wrinkle-forming strains vs max LNFD (cycles) are shown in Figure 8(a) and Figure 8(b) respectively.

The plots in Figure 8 clearly indicate a significantly greater correlation between the wrinkle-forming strains and the total LNFD, compared to the correlation between the wrinkle-forming strains and pressure-cycling LNFD. Figure 8(a) also indicates the presence of two outliers (#02-016 and #10-297) from the strain vs LNFD correlation trend observed for the remaining 45 wrinkles. This is attributed to the incidence of high shear strains during the wrinkle-forming process which invariably results in larger relative net fatigue damage, even when the wrinkle-forming strains are relatively small. The effect of high shear strains is also indicated by the relatively high circumferential net fatigue damage (CNFD) values recorded for the same two features. The CNFD results for #02-016 and #10-297 are approximately 5090% and 4082%, respectively, times the average CNFD for all the remaining 45 features assessed in this report. An important consequence of relatively high CNFD is higher susceptibility to a high rate of fatigue damage; hence, even though wrinkles #02-016 and #10-297 have relatively low wrinkle-forming strain and DFDI, there is a higher likelihood that fatigue damage due to pressure cycling may be faster in both features, compared to other wrinkle features assessed in this report.

https://doi.org/10.52202/078572-0044

Table 2: Wrinkle features (ranked) – upper bound DFDI > 95%

Wrinkle ID	Max Strain	Fatigue results from: wrinkle forming + operating cycles (operating cycles only)			
		Max LNFD (%)	Max LRFL (years)	Max CNFD (%)	Max CRFL (years)
02_016	0.1567	2.84 (~0.0)	100++ (100++)	1.42 (~0.0)	100++ (100++)
10_297	0.0896	1.44 (~0.0)	100++ (100++)	1.14 (~0.0)	100++ (100++)
10_155	0.3408	1.34 (~0.0)	100++ (100++)	0.08 (~0.0)	100++ (100++)
19_251	0.3186	1.24 (~0.0)	100++ (100++)	0.08 (~0.0)	100++ (100++)
09_390	0.2899	1.09 (~0.0)	100++ (100++)	0.17 (~0.0)	100++ (100++)
14_151	0.2552	1 (~0.0)	100++ (100++)	0.03 (~0.0)	100++ (100++)
14_124	0.2915	0.98 (~0.0)	100++ (100++)	0.07 (~0.0)	100++ (100++)
14_139	0.2915	0.97 (~0.0)	100++ (100++)	0.08 (~0.0)	100++ (100++)

Notes:
1. *These results assume sound pipe microstructure with no coinciding manufacturing features.*
2. *~0 means negligible*

Integrity Dig Recommendations vs CSA Z662

For this pipeline, CSA Z662 Clause 10.10.8.3 b) i) considers an acceptable wrinkle to be one whose height/pipe outside diameter (h/OD) ratio is ≤0.02. The lowest h/OD ratio measured was 0.026, meaning that all 47 wrinkles are considered defects requiring assessment and potential repair according to CSA Z662.

Using the process described in this paper, dig recommendations were based on exceedances of lower bound DFDI (≥80%), max LNFD (≥1.00%) and/or max CNFD (≥1.00%). These represent all features identified as medium-to-high risk of cracks being present. While the calculated fatigue life was found to be acceptable for all features, the decision to dig was based on the likelihood of cracks being present, even if they had acceptable remaining life. A total of 8 digs were recommended with the remainder recommended for continued monitoring by ILI. By utilizing this assessment process, ATCO was able to reduce its dig requirements by approximately 83% while maintaining confidence that the wrinkles remaining in service are safe under current operating conditions.

https://doi.org/10.52202/078572-0044

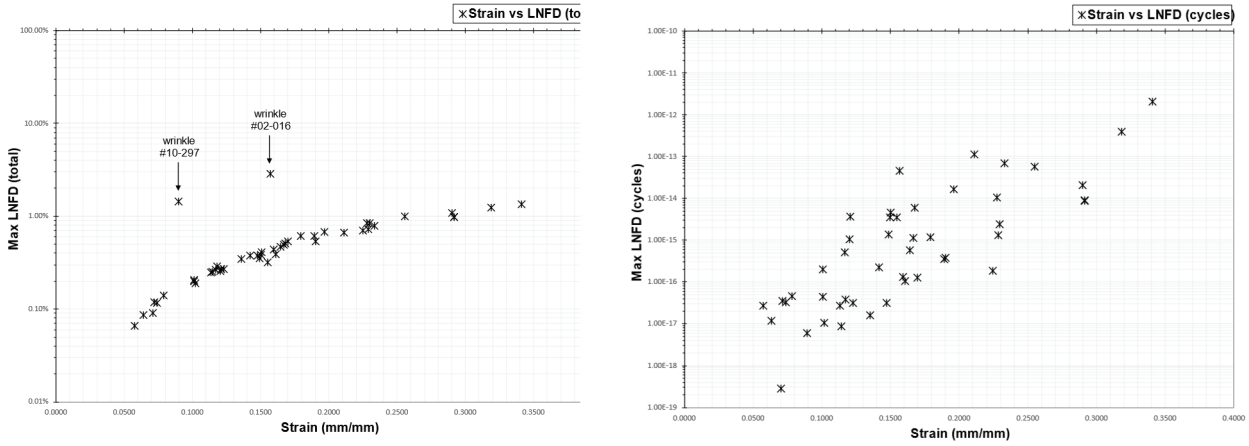

Figure 8. Correlation between wrinkle-strain and net fatigue damage

Conclusion

The strain-life fatigue evaluation performed in this paper shows that all 47 wrinkles satisfy the Level 3 fatigue damage and remaining life assessment criteria specified by API-579 2021. While the NFD results recorded for wrinkle #02-016 and wrinkle #10-297 are both considerably less than the NFD limit of 100% specified by API 579-2021, there exists a high chance of accelerated fatigue damage under pressure-cycling loading conditions or additional moment-loading conditions. This is attributed to the higher prevalence of shear strains in both wrinkles, as evidenced by the simultaneously high NFD of both wrinkles in both the longitudinal and circumferential directions. The NFD results for both wrinkles (#02-016 and #10-297) are also observed to be uncorrelated with the general trend between the wrinkle-forming strain/DFDI and the NFD.

Based on the DFDI criteria specified by API RP 1183, six features (#09-390, #10-155, #14-124, #14-139, #14-151, #19-251) are categorized as medium-to-high risk. These are features that recorded a DFDI close to (or greater than) 100% and as such, are considered the most susceptible to crack initiation, especially in the event of any additional loading conditions (such as unexpected ground movements) that may worsen the current strain state of the wrinkles. Magnetic particle inspection performed on some recent cut-outs showed evidence of manufacturing defects on the external surface of the pipe around the regions close to the wrinkle apex. There was however no indication of active fatigue crack growth (possibly due to hot wrinkle forming, as lab evidence shows) or environmental degradation mechanisms in the inspected cut-outs. The DFDI assumes that the microstructure of the pipe is free from imperfections and may therefore underestimate the true extent of strain damage during wrinkle formation.

https://doi.org/10.52202/078572-0044

8 digs were recommended based on DFDI, LNFD and CNFD exceedances. This represents a reduction in necessary digs of 83% relative to what would have been needed by only using the screening criterion from CSA Z662 Clause 10.10.8.3.

Acknowledgments

The authors would like to acknowledge Jonathan Prescott of Pacific Northern Gas (formerly of Stantec) for his contributions to the analysis method used in this paper while working at Stantec.

References

[1] API 579-1 / ASME FFS-2, 2021, Fitness-For-Service
[2] API RP 1183-2021, Assessment and Management of Pipeline Dents